Accepted Manuscript

5-Hydroxypyrido[2,3-*b*]pyrazin-6(5*H*)-one derivatives as novel dual inhibitors of HIV-1 reverse transcriptase-associated ribonuclease H and integrase

Lin Sun, Ping Gao, Guanyu Dong, Xujie Zhang, Xiqiang Cheng, Xiao Ding, Xueshun Wang, Dirk Daelemans, Erik De Clercq, Christophe Pannecouque, Luis Menéndez-Arias, Peng Zhan, Xinyong Liu

Please cite this article as: L. Sun, P. Gao, G. Dong, X. Zhang, X. Cheng, X. Ding, X. Wang, D. Daelemans, E. De Clercq, C. Pannecouque, L. Menéndez-Arias, P. Zhan, X. Liu, 5-Hydroxypyrido[2,3-*b*]pyrazin-6(5*H*)-one derivatives as novel dual inhibitors of HIV-1 reverse transcriptase-associated ribonuclease H and integrase, *European Journal of Medicinal Chemistry* (2018), doi: 10.1016/j.ejmech.2018.06.036.

7a
$IC_{50}^{RNase\ H}$ = 1.77 µM
IC_{50}^{IN} = 1.18 µM
ratio = 1.50

RNase H

Integrase

5-Hydroxypyrido[2,3-*b*]pyrazin-6(5*H*)-One Derivatives as Novel Dual Inhibitors of HIV-1 Reverse Transcriptase-Associated Ribonuclease H and Integrase

Lin Sun[a], Ping Gao[a], Guanyu Dong[a], Xujie Zhang[a], Xiqiang Cheng[a], Xiao Ding[a], Xueshun Wang[a], Dirk Daelemans [b], Erik De Clercq[b], Christophe Pannecouque[b,*], Luis Menéndez-Arias[c,*], Peng Zhan[a,*], Xinyong Liu[a,*]

[a]Department of Medicinal Chemistry, Key Laboratory of Chemical Biology, Ministry of Education, School of Pharmaceutical Sciences, Shandong University, Ji'nan, 250012

[b]Rega Institute for Medical Research, K.U.Leuven, Minderbroedersstraat 10, B-3000 Leuven, Belgium

[c]Centro de Biología Molecular "Severo Ochoa" (Consejo Superior de Investigaciones Científicas & Universidad Autónoma de Madrid), Madrid, Spain

[*]E-mails: christophe.pannecouque@rega.kuleuven.be (Pannecouque C.); lmenendez@cbm.csic.es (Menéndez-Arias L.); zhanpeng1982@sdu.edu.cn (Zhan P.); xinyongl@sdu.edu.cn (Liu X.Y.)

Abstract:

We reported herein the design, synthesis and biological evaluation of a series of 5-hydroxypyrido[2,3-*b*]pyrazin-6(5*H*)-one derivatives as HIV-1 reverse transcriptase (RT) ribonuclease H (RNase H) inhibitors using a privileged structure-guided scaffold refining strategy. In view of the similarities between the pharmacophore model of RNase H and integrase (IN) inhibitors as well as their catalytic sites, we also performed IN inhibition assays. Notably, the majority of these derivatives inhibited RNase H and IN at micromolar concentrations. Among them, compound **7a** exhibited similar inhibitory activity against RNase H and IN ($IC_{50}^{RNase\ H}$ = 1.77 μM, IC_{50}^{IN} = 1.18 μM, ratio = 1.50). To the best of our knowledge, this is the first reported dual

HIV-1 RNase H-IN inhibitor based on a 5-hydroxypyrido[2,3-*b*]pyrazin-6(5*H*)-one structure. Molecular modeling has been used to predict the binding mode of **7a** in complex with the catalytic cores of HIV-1 RNase H and IN. Taken together these results strongly support the feasibility of developing HIV-1 dual inhibitors from analog-based optimization of divalent metal ion chelators. Recently, the identification of dual inhibitors proved to be a highly effective strategy for novel antivirals discovery. Therefore, these compounds appear to be useful leads that can be further modified to develop more valuable anti-HIV-1 drugs with drug-like profiles.

Keywords: HAART; HIV-1 dual inhibitors; HIV-1 IN; RNase H; 5-hydroxypyrido[2,3-*b*]pyrazin-6(5*H*)-one derivatives; privileged structure

1. Introduction

Acquired immunodeficiency syndrome (AIDS) still remains one of the most severe public health challenges worldwide. The human immunodeficiency virus type 1 (HIV-1) is the etiological agent responsible for the disease [1]. Highly active antiretroviral therapy (HAART), including antivirals with different targets and mechanisms, has transformed the AIDS into a chronic disease [2]. However, the long duration of HAART treatments poses important risks such as the emergence of drug-resistant variants [3, 4], drug-drug interactions, and serious long-term toxicity [5]. Therefore, the search for novel anti-HIV-1 agents acting on new targets or on several targets simultaneously is urgent and essential [6].

The HIV-1 RT is a validated biological target for the treatment of AIDS and the most important target in current antiretroviral therapies. RT is a multifunctional enzyme with multiple activities, such as RNA- and DNA-dependent DNA polymerase, strand displacement synthesis, strand transfer, and RNase H [7]. However, only drugs targeting the RT-associated DNA polymerase function have been approved for clinical use. The RNase H activity plays a critical role in HIV-1 replication, by degrading the RNA strand in RNA-DNA hybrids generated during the reverse transcription. The RNase H active site features a highly conserved DEDD motif containing four

carboxylate residues D443, E478, D498 and D549, which could chelate two catalytic Mg^{2+} ions [8]. To date, even though none of the RNase H inhibitors has been approved for the treatment of HIV, the continued discovery and development of RNase H inhibitors led to the identification of a few chemotypes targeting the RNase H active site (**Figure 1**). The relevant structures are hydroxyisoquinolinedione (HID) [9], β-thujaplicinol (BPT) [10], diketoacid (DKA) [11], pyrimidinol carboxylic acid [12], naphthyridinone [13], pyridopyrimidinone [14], hydroxypyrimidine [15], hydroxylisoquinoline [16], and hydroxypyridonecarboxylic acid [17]. All those chemotypes contain a coplanar chelating triad that competitively binds to the divalent cations in the RNase H active site. Those compounds having a terminal biaryl substituent proved to be much more effective, while sharing a similar pharmacophore "T" conformation.
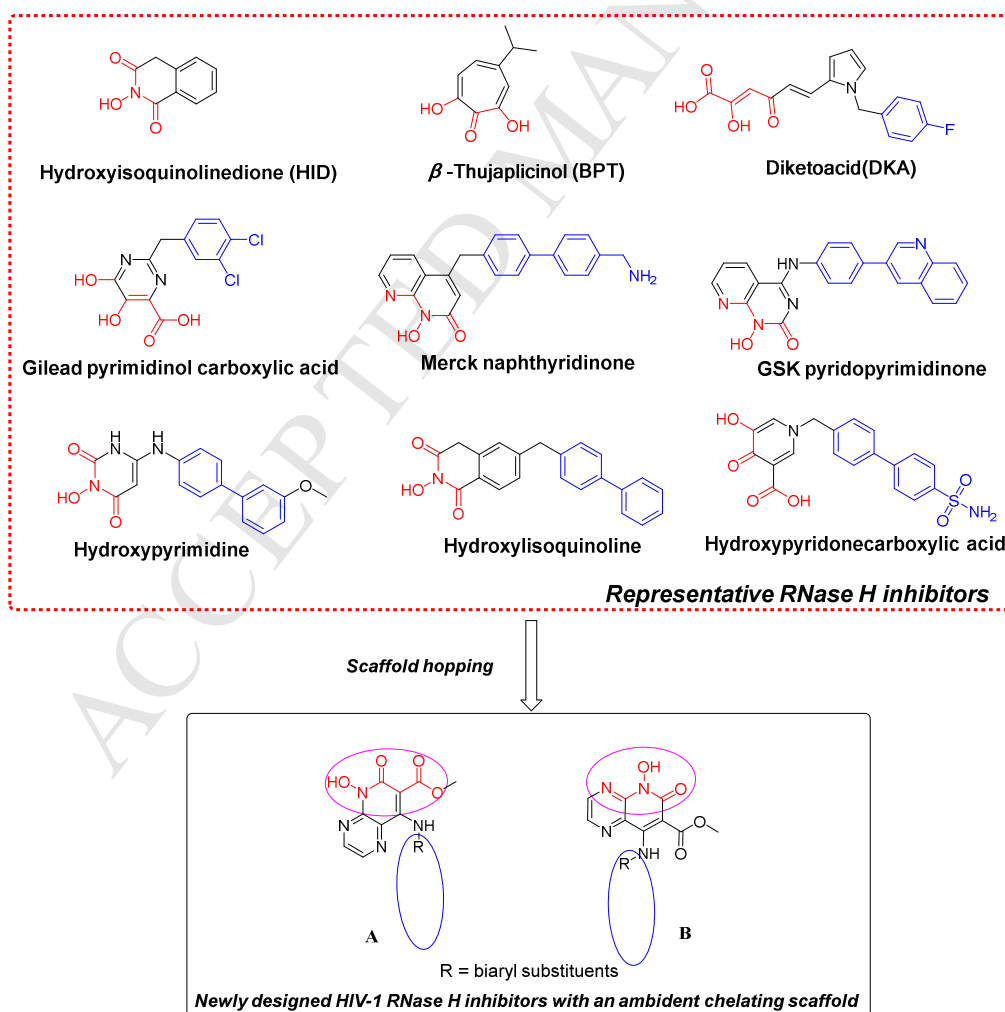
Figure 1. Structures of the representative RNase H inhibitors and schematic illustration of the

scaffold hopping-based small-molecule library design procedure derived from an ambient scaffold (with two different chelating configurations: **A** and **B**) described in this work (by alternative privileged motifs and modifying branching moieties in the known active molecules). Each inhibitor features a chelating triad (red) and a terminal hydrophobic aryl group (blue).

We report herein the design of the 5-hydroxypyrido[2,3-*b*]pyrazin-6(5*H*)-one scaffold as an ambient chelating core using a scaffold hopping strategy in medicinal chemistry (**Figure 1**). In addition, we selected different biaryl substituents from potent RNase H inhibitors to construct a small library of 5-hydroxypyrido[2,3-*b*]pyrazin-6(5*H*)-one derivatives. Key to this design is the introduction of biaryl substituents at C-4 position through a NH linker to keep the "T" conformation, with the goal of achieving RNase H inhibition.

Besides, numerous divalent metal ion chelators were recently identified as miscellaneous inhibitors targeting bridged dinuclear metalloenzymes, indicating that such chemotypes have a wide range of biological activities [18-20]. Like the RNase H, the HIV-1 integrase (IN) is a metalloenzyme with an important function in the viral life cycle. It catalyzes the integration of the viral DNA into the genome of infected host cells by the coordinated action of two enzyme activities. First, IN catalyzes a 3'-end processing (3'-P) reaction on the proviral DNA, and second, it facilitates strand-transfer (ST) to complete the integration process [21]. Three highly conserved catalytic residues in the catalytic core domain (CCD), namely, D64, D116, and E152 (DDE motif) coordinate the two divalent cations necessary for the ST function [22]. The catalytic domains of the HIV-1 IN and RNase H share a similar folding, composed of a central five-stranded mixed *β*-sheet flanked by several *α*-helices, and having a similar topology [23]. The geometries of the catalytic sites of HIV-1 RNase H and IN are similar, with their active site residues and magnesium ions located at structurally equivalent positions in both enzymes [24]. Up to now, there are four strand transfer IN inhibitors (INSTIs) approved by the U. S. Food and Drug Administration (FDA) (**Figure 2**). These drugs are raltegravir (RAL) [25], elvitegravir (EVG) [26], dolutegravir (DTG) [27], and bictegravir [28]. All of them

share similar structural features with RNase H inhibitors, including the coplanar triad of heteroatoms and a terminal hydrophobic aryl moiety.

Therefore, based on the overlapping pharmacophore features shown by HIV-1 RNase H and IN inhibitors, we also determined the inhibitory activity of 5-hydroxypyrido[2,3-b]pyrazin-6(5H)-one derivatives in IN ST assays. We describe herein the chemical synthesis and biochemical evaluation of these newly designed derivatives.
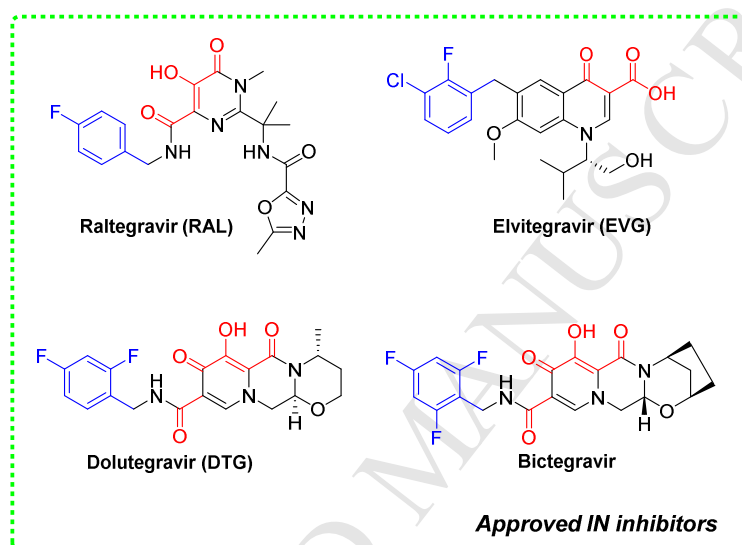
Figure 2. Structures of U. S. FDA-approved INSTIs, each features a chelating triad (red) and a terminal hydrophobic aryl group (blue).

2. Results and discussion

2.1. Chemistry

The target compounds **7a**-**7k** were prepared *via* a concise synthetic route as outlined in **Scheme 1** [29]. Commercially available methyl 3-chloropyrazine-2-carboxylate (**1**) was treated as the primary starting material to produce all derivatives using well-established methods. Treating with benzoxylamine in DMSO and DIPEA to give **2**, followed by an acylation with methyl 3-chloro-3-oxopropanoate yielded the intermediate **3**. Ring closure of **3** by reacting with sodium methoxide in methanol solution to produce the cyclized product **4**. This heterocyclic scaffold was then tosylated with toluenesulfonyl chloride to obtain intermediate **5**. Subsequent reaction with corresponding amines to generate **6a**-**6k**.

Finally, the desired compounds were obtained by a hydrogenolytic deprotection of the *N*-hydroxyl group.
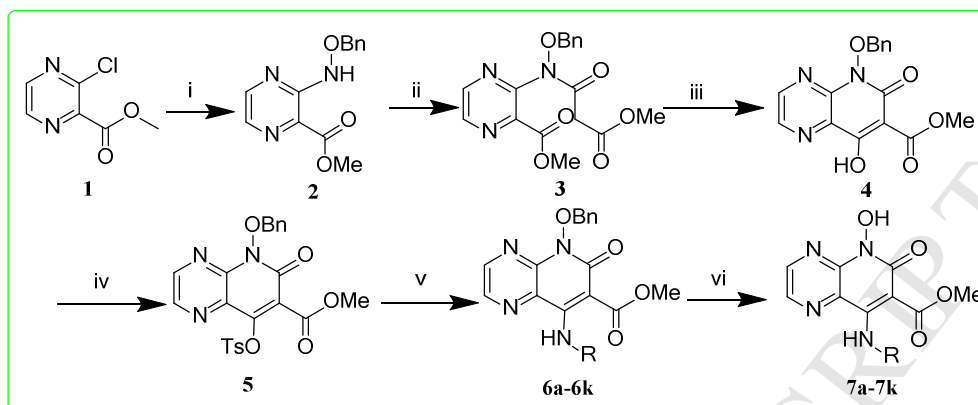
Scheme 1. Reagents and conditions: i) BnONH$_2$, DIPEA, DMSO, Mw 100 °C; ii) ClCOCH$_2$COOCH$_3$, TEA, DCM, 0 °C to 45 °C; iii) MeOH, MeONa, r.t.; iv) TsCl, DIPEA, MeCN, DCM, r.t.; v) Corresponding diaryl amine, DIPEA, DMF, 50 °C; vi) H$_2$, 10% Pd•C, DCM, MeOH, r.t..

2.2. Biological activity

Table 1. Anti-RNase H, anti-IN, antiviral activities and cytotoxicity of compounds **7a**-**7k**.

Compds	R	IC$_{50}$ (µM)		ratio[c]	EC$_{50}$ (µM)[d]	CC$_{50}$ (µM)[e]
		RNase H[a]	IN[b]			
7a		1.77 ± 0.62	1.18 ± 0.37	1.50	> 0.34	0.34 ± 0.05
7b		5.56 ± 1.29	22.80 ± 6.10	0.24	> 1.19	1.19 ± 0.10
7c		13.32 ± 2.34	> 25		> 5.68	5.68 ± 1.31
7d		4.02 ± 1.02	0.25 ± 0.01	16.08	> 1.16	1.16 ± 0.12
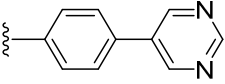
	Structure	a	b	c	d	e
7e		3.24 ± 0.92	1.49 ± 0.27	2.17	> 8.04	8.04 ± 0.79
7f		1.85 ± 0.60	10.85 ± 2.22	0.17	> 5.89	5.89 ± 1.02
7g		5.90 ± 1.35	> 25		> 1.47	1.47 ± 0.11
7h		4.72 ± 1.17	0.22 ± 0.04	21.45	> 1.32	1.32 ± 0.33
7i		4.30 ± 1.20	> 25		> 1.38	1.38 ± 0.14
7j		5.11 ± 1.29	6.74 ± 1.57	0.76	> 7.15	7.15 ± 0.94
7k		5.25 ± 0.81	> 25		> 7.00	7.00 ± 0.49
BPT		2.50 ± 0.78				
RAL			0.20 ± 0.05		$(1.17 \pm 0.36) \times 10^{-2}$	>56.25
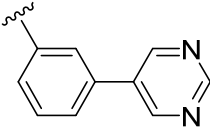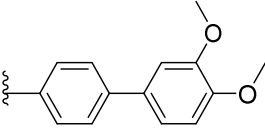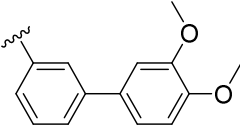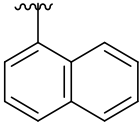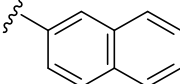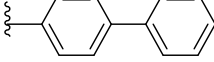
[a]Concentration required to inhibit by 50% the in vitro RNase H activity.

[b]Concentration required to inhibit by 50% the in vitro overall IN activity.

[c]$IC_{50}^{RNase\ H}/IC_{50}^{IN}$ ratio.

[d]Concentration of compound required to achieve 50% protection of MT-4 cell cultures against HIV-1-induced cytotoxicity, as determined by the MTT method.

[e]Concentration required to reduce the viability of mock-infected cell cultures by 50%, as determined by the MTT method.

2.2.1. Inhibition of HIV-1 RNase H activity

All newly synthesized compounds **7a**-**7k** were tested *in vitro* for their inhibition

ability to RNase H function of HIV-1 RT and results were analyzed by denaturing polyacrylamide gel electrophoresis [30]. In general, **7a**-**7k** were all potent RNase H inhibitors with IC_{50} values ranging from 1.77 – 13.32 µM (**Table 1**). Compounds **7a** and **7f** were the most active derivatives of this series, with IC_{50} values of 1.77 and 1.85 µM, respectively, slightly more potent than the reference compound *β*-thujaplicinol (BPT) (IC_{50} = 2.50 µM). The least potent compound was **7c** (IC_{50} value of 13.32 µM), in which the 4-CN phenyl of **7a** was replaced by a 3-CN phenyl moiety, causing a reduction of one order of magnitude in RNase H inhibition.

Among the *para*-substituted benzene derivatives (**7a**, **7c**, **7e**, **7g**, **7k**), taking the least substituted compound **7k** (IC_{50} value of 5.25 µM) as reference, substitution of the phenyl on the C-4 of the benzene ring (**7k**) with a 4-CN phenyl (**7a**) or a 5-pyrimidyl group (**7e**), lead to 3.0 and 1.6-fold increases in RNase H inhibitory activity, respectively. However, the replacement of the phenyl on the C-4 of the benzene ring (**7k**) with 3,4-diOCH$_3$ phenyl (**7g**) or 3-CN phenyl (**7c**) groups, decreased their RNase H inhibitory activity. The order of potency of the *para*-substitutions was as follows: 4-CN phenyl (**7a**) > 5-pyrimidyl (**7e**) > phenyl (**7k**) > 3,4-diOCH$_3$ phenyl (**7g**) > 3-CN phenyl (**7c**).

While within the *meta*-substituted benzene derivatives, the 4-CN phenyl derivative (**7b**, IC_{50} value of 5.56 µM) was the least active compound. When the 4-CN phenyl on the C-3 of the benzene ring (**7b**) was replaced with a 5-pyrimidyl (**7f**, IC_{50} value of 1.85 µM), 3-CN phenyl (**7d**, IC_{50} value of 4.02 µM) and 3,4-diOCH$_3$ phenyl (**7h**, IC_{50} value of 4.72 µM), potencies were increased 3, 1.4 and 1.2 times, respectively. The order of potency of the *meta*-substitutions was as follows: 5-pyrimidyl (**7f**) > 3-CN phenyl (**7d**) > 3,4-diOCH$_3$ phenyl (**7h**) > 4-CN phenyl (**7b**).

The shift of the 3-CN phenyl from position 4 (**7c**) to 3 of the benzene gave **7d**, causing a 3.3-fold increase in anti-RNase H activity. Interestingly, the same trend was also observed when the groups in position 4 of the benzene (**7e**, **7g**) were shifted to position 3 (**7f**, **7h**), inhibitory activities increased in 1.8, 1.3-fold, respectively. However, the 4-CN phenyl shifted from position 4 (**7a**) to 3 of the benzene gave **7b**, leading to a 3.1-fold decrease in RNase H inhibitory activity. As for the naphthyl

derivatives, the 1-naphthyl derivative (**7i**, IC_{50} value of 4.30 μM) proved to be slightly better than 2-naphthyl (**7j**, IC_{50} value of 5.11 μM).

The structure-activity relationships (SARs) analysis based on the results obtained showed that: i) The *meta*-substituted benzene derivatives proved to be more effective than *para*-substituted benzene ones; ii) among the *para*-substituted benzene derivatives, the CN position has a significantly different effect in RNase H inhibition (exemplified by **7a** and **7c**), while the introduction of an electron donor methoxy group has little influence in its anti-RNase H potency (exemplified by **7g** and **7k**).

2.2.2. Inhibition of HIV-1 IN activity

The IN inhibitory activities of all newly synthesized 5-hydroxypyrido[2,3-*b*]pyrazin-6(5*H*)-one derivatives were determined by using an ELISA method [31]. The obtained IC_{50} values are shown in **Table 1**.

Among all analogues, **7d** and **7h** were the most active compounds of this series, with remarkable IN inhibitory activity in submicromolar level (IC_{50} value of 0.25, 0.22 μM, respectively), comparable to the reference drug **RAL** (IC_{50} value of 0.20 μM). In striking contrast, four compounds (**7c**, **7g**, **7i**, **7k**) were considered to be almost inactive (IC_{50} values of > 25 μM). The remaining five compounds (**7a**, **7b**, **7e**, **7f**, **7j**) were moderate IN inhibitors since their IC_{50} values ranged from 1.18 to 22.80 μM.

Among the *para*-substituted benzene analogues (**7a**, **7c**, **7e**, **7g**, **7k**), the most active one was the 4-CN phenyl derivative (**7a**) with an IC_{50} value of 1.18 μM. The replacement of the 4-CN phenyl on the C-4 of the benzene ring (**7a**) with a 5-pyrimidyl (**7e**, IC_{50} value of 1.49 μM), resulted in a 1.3-fold reduction of the observed inhibition. The same behaviour had been also observed in RNase H inhibition assays. However, the other three derivatives (**7c**, **7g**, **7k**) were found inactive even up to 25 μM. The order of potency of the *para*-substituted benzene derivatives was as follows: 4-CN phenyl derivative (**7a**) > 5-pyrimidyl (**7e**) > > 3-CN phenyl (**7c**), 3,4-diOCH$_3$ phenyl (**7g**), phenyl (**7k**).

Within the *meta*-substituted benzene derivatives (**7b**, **7d**, **7f**, **7h**), **7h** and **7d** were found to be the most active compounds. The substitution of the 3,4-diOCH$_3$ phenyl on

the C-3 of the benzene ring (**7h**) with 5-pyrimidyl (**7f**, IC_{50} value of 10.85 μM), and 4-CN phenyl (**7b**, IC_{50} value of 22.80 μM), led to a loss of inhibitory activity that was estimated in 49.3 and 103.6 times for compounds **7f** and **7b**, respectively. Interestingly, **7b** was also the least active compound of the *meta*-substituted benzene series in RNase H inhibition assays. The IN inhibitory potency of the *meta*-substituted benzene derivatives followed the order: 3,4-diOCH$_3$ phenyl (**7h**) > 3-CN phenyl (**7d**) > 5-pyrimidyl (**7f**) > 4-CN phenyl (**7b**).

The shift of the 3-CN phenyl from position 3 (**7d**, **7h**) to 4 of the benzene gave the corresponding compounds (**7c**, **7g**) that almost lost the IN inhibitory activity. However, the shift of the 4-CN phenyl from position 3 (**7b**) to 4 of the benzene gave a compound (**7a**) showing a significantly increased (19.3-fold) inhibitory activity. The same trend was also seen when the substitution in C-3 position (**7f**) of the benzene was shifted to C-4 position (**7e**), leading to a 7.3-fold increase in inhibitory activity. As for the naphthyl derivatives, the 2-naphthyl (**7j**, IC_{50} value of 6.74 μM) showed much higher potency than the 1-naphthyl derivative (**7i**, IC_{50} value of > 25 μM).

Analysis of SARs in inhibiting HIV-1 IN revealed that: i) generally, *meta*-substituted benzene derivatives were better inhibitors than the *para*-substituted benzene compounds, as exemplified by **7d** and **7h**; ii) among the *para*-substituted benzene derivatives, the 4-CN phenyl substitution rendered more potent drugs than the 3-CN phenyl group, while the opposite was true for *meta*-substituted benzene derivatives.

Compounds with low $IC_{50}^{RNase\ H}/IC_{50}^{IN}$ ratio (~ 1) indicate that they have the suitable balance in inhibiting RNase H and IN, and could be considered as efficient inhibitors of both targets [32, 33]. As shown in **Table 1**, it is worth noting that **7a**, **7e** and **7j**, with the ratio values of 1.50, 2.17 and 0.76, respectively, were deemed to be dual RNase H-IN inhibitors. Concerning the superior inhibition activities of **7a** in blocking both targets, there's no doubt that **7a** is best dual inhibitor of this series. A concise SARs analysis of the three dual inhibitors showed that although **7j** featured the lowest ratio (0.76) among the dual inhibitors, the naphthyl derivative (**7j**) proved to be less effective than inhibitors having biphenyl groups (**7a**, **7e**).

2.2.3. *In vitro* anti-HIV assay

All the derivatives were tested for their antiviral activity and cytotoxicity using MT-4 cells infected by HIV-1 (strain III_B). EC_{50} and CC_{50} values for compounds **7a**-**7k** were shown in **Table 1**. **RAL** was used as the reference drug. Unfortunately, none of tested compounds inhibited HIV-1 replication in cell culture at the highest tested concentrations, hindering their potential application as antiviral drugs.

As shown in **Table 1**, among the newly synthesized series, the best RNase H inhibitor **7a** and the best IN inhibitor **7h**, showed the relatively highest cytotoxicity, with CC_{50} values of 0.34 and 1.32 μM, respectively. An investigation of structure-cytotoxicity relationships (SCRs) reveals that: i) when the terminal aromatic group was fixed, the cytotoxicity of the *meta*-substituted benzene derivatives proved to be higher than that of *para*-substituted benzene ones (exemplified by **7c** and **7d**); while ii) 5-pyrimidyl derivatives (**7e**, **7f**) showed minimal cytotoxicity in each group.

The results of cytotoxicity tests revealed that these compounds might not only target HIV-1 metalloenzymes (IN and RNase H), but human metalloenzymes as well, indicating that selectivity between virus enzymes and human cellular targets should be improved through systematic and precise drug design in future drug optimization.

2.2.4. Molecular Docking
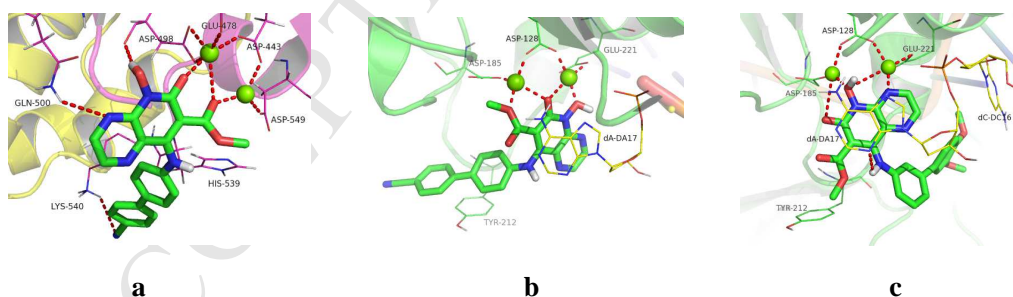
Figure 3. Predicted binding modes of **7a** (green) in the HIV-1 RNase H active site (**a**, PDB code: 5J1E) and PFV IN active site (**b**, PDB code: 3OYA). Predicted binding mode of **7h** (green) in the PFV IN active site (**c**, PDB code: 3OYA). Amino acid residues important for ligand binding are represented in lines. Magnesium ions are depicted as green spheres. Chelating and H-bond interactions are indicated by red dashed lines. Hydrogens (nonpolar) are not shown. Figures were prepared with the PyMOL visualization program (http://www.pymol.org).

For a better interpretation of SAR of **7a** ($IC_{50}^{RNase\ H}$ = 1.77 µM，IC_{50}^{IN} = 1.18 µM, ratio = 1.50), considered as the best RNase H inhibitor of the series, as well as the most effective dual RNase H-IN inhibitor, we performed molecular docking studies using the software SurflexDock Sybyl-X 2.0.

As shown in **Figure 3a**, the predicted binding mode of compound **7a** in the RNase H active site suggests an interaction between the chelating core (in configuration **A**, **Figure 1**) and the two divalent catalytic metal cations, which are coordinated to catalytic residues D443, E478, D498, and D549 (PDB code: 5J1E). The hydroxyl group at the 5-position of **7a** can form an H-bonding interaction with the carbonyl group of D498, while the nitrogen atom at 4-position of **7a** can make another hydrogen bond with the amino group of Q500. These interactions would position **7a** close to the active site. Besides, additional H-bonding was established between the CN group at the terminal of biaryl substituent and the amino group of K540, also essential for RNase H inhibition. The flexible NH moiety at the 8-position of the scaffold introduces conformational flexibility and allows the establishment of π-π interactions between the biphenyl moiety of **7a** and the imidazole ring of the highly conserved residue H539. This interaction restricts the conformational flexibility of H539 and therefore has an influence on the catalytic efficiency of the RNase H. The predicted molecular model was consistent with the mechanism of active site inhibition.

In the absence of a crystal structure of full-length HIV IN, we used the prototype foamy virus (PFV) IN as a reliable model of the HIV IN active site [34, 35]. The obtained model for PFV IN in complex with **7a** was constructed by using the PDB structure 3OYA. As shown in **Figure 3b**, the model predicts chelating interactions between our chemotype core (in configuration **A**) and the two magnesium ions which are coordinated by conserved residues (D128, D185, E221) in the PFV IN active site, corresponding to the D64, D116, and E152 in the HIV-1 IN catalytic core, respectively. In addition, the conserved terminal 3′-deoxyadenosine 17 in the DNA also stacks with the chelating core of our scaffold, as it does for approved INSTIs. Furthermore, the terminal biaryl substituent could participate in π-stacking

interactions with the benzene ring of Y212. These interactions seem to be of vital importance for the IN inhibitory potency of **7a**.

For a better understanding of how these derivatives interact with the IN active site, we also performed docking analysis of **7h** (the best IN inhibitor in our series) in complex with PFV IN (PDB code: 3OYA). As shown in **Figure 3c**, the binding pattern of **7h** is different from that of **7a**. First, the metal chelating core acts in configuration **B** (**Figure 1**), not **A**. Second, the methoxy at position 7 could make stacking interactions with the benzene ring of Y212, while the terminal biaryl substituent showed T-stacking interactions with the pyrimidine ring of cytosine 16 in the DNA substrate. In addition, the chelating core maintains the π-π interaction with the purine ring of adenosine 17 in the DNA substrate. An additional H-bonding interaction was predicted for the NH linker at position 8 and the purine ring of adenosine 17.

These docking analysis are consistent with the experimental observations showing that **7a** is a potent HIV-1 RNase H-IN dual inhibitor, validating the advantages of ambident scaffolds in metal ion chelating. These findings will provide a basis for further rational drug optimization in the future.

3. Conclusion

In this study, we have designed, synthesized, and evaluated a novel series of 5-hydroxypyrido[2,3-*b*]pyrazin-6(5*H*)-one derivatives as RNase H inhibitors with an ambident chelating core. In addition, concerning the similarities between the pharmacophore model of RNase H and INST inhibitors as well as their catalytic sites, we also performed their inhibitory assay on recombinant IN. The results showed that most of the newly designed compounds exhibited potent inhibitory activity against RNase H and IN.

Among all analogues, **7a** and **7f** were the most remarkable RNase H inhibitors of this series (IC$_{50}$ values of 1.77 and 1.85 µM, respectively), slightly more potent than the control drug *β*-thujaplicinol (**BPT**) (IC$_{50}$ value of 2.50 µM). Compounds **7d** and **7h** exhibited the most prominent IN inhibitory activity (IC$_{50}$ values of 0.25 and 0.22 µM, respectively), similar to that shown by a reference approved drug such as

raltegravir (**RAL**) (IC_{50} value of 0.20 μM). The best dual inhibitor **7a** in blocking RNase H and IN achieved suitable balanced micromolar inhibition ($IC_{50}^{RNase\ H}$ = 1.77 μM，IC_{50}^{IN} = 1.18 μM, ratio = 1.50), validating the feasibility of identifying dual HIV-1 RNase H-IN inhibitors through the modification of chelating privileged structures. The analyses of SARs and SCRs are expected to offer beneficial guidance for further rational optimization. Molecular modeling also predicted the possible binding patterns of dual RNase H-IN inhibitor with the ambident chelating scaffold. Regrettably, none of novel compounds inhibited HIV replication when performed in MT-4/MTT assays, while their high cytotoxicity could be related to a lack of selectivity of these metal binding compounds against host metalloenzymes. Therefore, improved druggability and selectivity of these derivatives are future research goals.

Currently, the development of dual inhibitors is an innovative approach to improve the efficiency of HAART therapies [6]. Dual inhibitors have been reported to play an important role in the treatment of several diseases (e.g. Alzheimer [36], Parkinson [37], inflammation [38], and cancer [39]). In the field of anti-HIV drug research, HIV-1 IN and RNase H represent very attractive pharmacological targets, and the development of HIV-1 dual RNase H-IN inhibitors is expected to be a highly effective strategy with more therapeutic benefit [22]. Consequently, **7a**, the best dual inhibitor of this series, could serve as a lead for further modification to get more potent dual RNase-IN inhibitors, of important practical significance.

4. Experimental Section

4.1. Chemistry

^{1}H NMR and ^{13}C NMR spectra were recorded on a Bruker AV-400 spectrometer using solvents as indicated (DMSO-d_6). Chemical shifts were reported in δ values (ppm) with tetramethylsilane as the internal reference, and J values were reported in hertz (Hz). Melting points (mp) were determined on a micromelting point apparatus. TLC was performed on Silica Gel GF254 for TLC (Merck) and spots were visualized by iodine vapor or by irradiation with UV light (λ = 254 nm). Flash column chromatography was performed on column packed with Silica Gel60 (200-300 mesh).

Thin layer chromatography was performed on pre-coated

HUANGHAI_HSGF254, 0.15-0.2 mm TLC-plates. Solvents were of reagent grade and were purified and dried by standard methods when necessary. Concentration of the reaction solutions involved the use of rotary evaporator at reduced pressure. The solvents of CH_2Cl_2, Et_3N and methanol etc. were obtained from Sinopharm Chemical Reagent Co., Ltd (SCRC), which were of AR grade. The key reactants including 3-chloro-3-oxopropanoate, methyl 3-chloropyrazine-2-carboxylate, 4-methylbenzene-1-sulfonyl chloride, *O*-benzylhydroxylamine etc. were purchased from Bide Pharmatech Co. Ltd.

4.1.1. General procedure for the synthesis of methyl 3-((benzyloxy)amino)pyrazine-2-carboxylate (**2**)

A mixture of **1** (504 mg, 2.9 mmol) and *O*-benzylhydroxylamine (1073 mg, 8.72 mmol) in diisopropylethylamine (1.44 mL, 8.72 mmol) was irradiated in microwave at 100 ℃ for 1 h. The reaction mixture was concentrated in vacuo and the residue was purified by silica gel chromatography using ethyl acetate and petroleum ether (1:4) as an eluent to provide **2** as a yellow solid in 16% yield, mp: 60-62 ℃. ^{1}H NMR (400 MHz, DMSO-d_6) δ 10.33 (s, 1H, N-H), 8.50 (d, J = 2.3 Hz, 1H, pyrazine-H), 8.13 (d, J = 2.3 Hz, 1H, pyrazine-H), 7.47 (dd, J = 8.2, 1.6 Hz, 2H, Ph-H), 7.42 – 7.33 (m, 3H, Ph-H), 4.96 (s, 2H, CH_2), 3.82 (s, 3H, CH_3). ^{13}C NMR (100 MHz, DMSO-d_6) δ 165.51, 155.09, 146.75, 136.19, 134.63, 128.69 (2×C), 128.30 (2×C), 128.18, 125.53, 76.85, 52.44. ESI-MS: m/z 260.3 (M+1), 282.4 (M+23). $C_{13}H_{13}N_3O_3$ [259.3].

4.1.2. General procedure for the synthesis of methyl 3-(*N*-(benzyloxy)-3-methoxy-3-oxopropanamido)pyrazine-2-carboxylate (**3**)

To a solution of **2** (1897 mg, 7.29 mmol) and triethylamine (2.02 mL, 14.59 mmol) in CH_2Cl_2 (40 mL) was added methyl 3-chloro-3-oxopropanoate (3.12 mL, 29.18 mmol) dropwise at 0 ℃, and the mixture was stirred at 45 ℃ (24 h). The mixture was then extracted (CH_2Cl_2) and washed sequentially with brine and dried (Na_2SO_4). The organic phase was filtered and concentrated, and the crude residue was purified by silica gel chromatography using ethyl acetate and petroleum ether (1:3) as an eluent to provide **3** as a yellow solid in 90% yield, mp: 81-82 ℃. ^{1}H NMR (400 MHz, DMSO-d_6) δ 8.80 (d, J = 2.3 Hz, 1H, pyrazine-H), 8.71 (d, J = 2.3 Hz, 1H,

pyrazine-H), 7.42 – 7.35 (m, 5H, Ph-H), 5.04 (s, 2H, CH$_2$), 3.81 (s, 3H, CH$_3$), 3.78 (s, 2H, CH$_2$), 3.63 (s, 3H, CH$_3$). ^{13}C NMR (100 MHz, DMSO-d_6) δ 166.82(2×C), 163.85, 145.65, 142.72, 140.07, 133.84, 129.68, 128.92 (2×C), 128.34, 77.76, 52.74, 52.08, 40.73. ESI-MS: m/z 360.2 (M+1), 382.3 (M+23), 398.4 (M+39). C$_{17}$H$_{17}$N$_3$O$_6$ [359.3].

4.1.3. General procedure for the synthesis of methyl 5-(benzyloxy)-8-hydroxy-6-oxo-5,6-dihydropyrido[2,3-b]pyrazine-7-carboxylate (**4**)

To a solution of **3** (212 mg, 0.557 mmol) in MeOH (10 mL) was added sodium methanolate (74 mg, 1.376 mmol) at room temperature, and the resulting suspension was stirred at room temperature (overnight). Acidification to pH 4 by the addition of aqueous 2 N HCl gave a precipitate, which was collected and dried to provide **4** as a white solid in 93% yield, mp: 195-197 ºC. ^{1}H NMR (400 MHz, DMSO-d_6) δ 8.88 (d, J = 2.3 Hz, 1H, pyrazine-H), 8.70 (d, J = 2.3 Hz, 1H, pyrazine-H), 7.64- 7.62 (m, 2H, Ph-H), 7.46-7.39 (m, 3H, Ph-H), 5.17 (s, 2H, CH$_2$), 3.84 (s, 3H, CH$_3$). ^{13}C NMR (100 MHz, DMSO-d_6) δ 164.33, 158.58, 156.48, 146.58, 144.82, 139.24, 134.32, 129.51 (2×C), 128.94, 128.37 (2×C), 127.15, 108.94, 77.78, 52.38. ESI-MS: m/z 328.4 (M+1), 350.4 (M+23). C$_{16}$H$_{13}$N$_3$O$_5$ [327.3].

4.1.4. General procedure for the synthesis of methyl 5-(benzyloxy)-6-oxo-8-(tosyloxy)-5,6-dihydropyrido[2,3-b]pyrazine-7-carboxylate (**5**)

To a suspension of **4** (101 mg, 0.306 mmol) in CH$_3$CN (6 mL) and CH$_2$Cl$_2$ (2 mL) were added diisopropylethylamine (0.303 mL, 1.834 mmol) and 4-methylbenzene-1-sulfonyl chloride (175 mg, 0.917 mmol), and the mixture was stirred at room temperature (overnight). The resulting mixture was purified by silica gel chromatography using ethyl acetate and petroleum ether (1:3) to provide **5** as a yellow solid in 75% yield, mp: 162-164 ºC. ^{1}H NMR (400 MHz, DMSO-d_6) δ 8.90 (d, J = 2.3 Hz, 1H, pyrazine-H), 8.64 (d, J = 2.3 Hz, 1H, pyrazine-H), 7.90 (d, J = 8.4 Hz, 2H, Ph-H), 7.64 (dd, J = 7.4, 2.0 Hz, 2H, Ph-H), 7.52 (d, J = 8.1 Hz, 2H, Ph-H), 7.47 – 7.43 (m, 3H, Ph-H), 5.24 (s, 2H, CH$_2$), 3.66 (s, 3H, CH$_3$), 2.46 (s, 3H, CH$_3$). ^{13}C NMR (100 MHz, DMSO-d_6) δ 161.10, 155.06, 149.49, 146.91, 146.51, 145.06, 140.90, 133.97, 132.08, 130.17 (2×C), 129.67 (2×C), 129.15, 128.49 (2×C), 128.47,

127.47 (2×C), 123.42, 78.12, 53.00, 21.25. ESI-MS: m/z 482.4 (M+1), 504.4 (M+23), 520.4 (M+39). $C_{23}H_{19}N_3O_7S$ [481.5].

4.1.5. General procedure for the synthesis of compounds **6a**-**6k**

A solution of **5** (1.454 mmol, 1 eq), diisopropylethylamine (4.362 mmol, 3 eq) and corresponding diaryl amine (2.181 mmol, 1.5 eq) in DMF (6 mL) was heated to 50 ºC (2 h). The mixture was then extracted (CH_2Cl_2) and washed sequentially with brine and dried (Na_2SO_4). The organic phase was filtered and concentrated, and the crude residue was purified by silica gel chromatography using MeOH and DCM (1:100) as an eluent to provide amides (**6a**−**6k**).

Methyl 5-(benzyloxy)-8-((4'-cyano-[1,1'-biphenyl]-4-yl)amino)-6-oxo-5,6-dihydropyrido[2,3-b]pyrazine-7-carboxylate (**6a**): yellow solid, yield 63%, mp: 225-226 ºC. ^{1}H NMR (400 MHz, DMSO-*d*6) δ 9.74 (s, 1H, N-H), 8.89 (d, *J* = 2.4 Hz, 1H, pyrazine-H), 8.68 (d, *J* = 2.4 Hz, 1H, pyrazine-H), 7.92 (s, 4H, Ph-H), 7.77 (d, *J* = 8.6 Hz, 2H), 7.66 – 7.64 (m, 2H, Ph-H), 7.47- 7.40 (m, 3H, Ph-H), 7.32 (d, *J* = 8.6 Hz, 2H, Ph-H), 5.18 (s, 2H, CH$_2$), 3.13 (s, 3H, CH$_3$). ^{13}C NMR (100 MHz, DMSO-*d*$_6$) δ 164.32, 156.97, 146.45, 144.99, 144.60, 143.84, 139.81, 138.51, 134.73, 134.48, 132.87 (2×C), 129.51 (2×C), 128.90, 128.37 (2×C), 127.42, 127.24 (2×C), 127.21 (2×C), 124.54 (2×C), 118.89, 109.82, 102.85, 77.65, 51.32. ESI-MS: m/z 504.4 (M+1), 526.5 (M+23), 542.5 (M+39). $C_{29}H_{21}N_5O_4$ [503.5].

Methyl 5-(benzyloxy)-8-((4'-cyano-[1,1'-biphenyl]-3-yl)amino)-6-oxo-5,6-dihydropyrido[2,3-b]pyrazine-7-carboxylate (**6b**): yellow solid, yield 59%, mp: 239-241 ºC. ^{1}H NMR (400 MHz, DMSO-*d*$_6$) δ 9.72 (s, 1H, N-H), 8.89 (d, *J* = 2.3 Hz, 1H, pyrazine-H), 8.68 (d, *J* = 2.3 Hz, 1H, pyrazine-H), 7.96 (d, *J* = 8.5 Hz, 2H, Ph-H), 7.88 (d, *J* = 8.5 Hz, 2H, Ph-H), 7.65 (dd, *J* = 7.7, 1.6 Hz, 2H, Ph-H), 7.59 (d, *J* = 8.0 Hz, 1H, Ph-H), 7.53 – 7.50 (m, 2H, Ph-H), 7.47 – 7.41 (m, 3H, Ph-H), 7.31 (d, *J* = 8.0 Hz, 1H, Ph-H), 5.18 (s, 2H, CH$_2$), 2.99 (s, 3H, CH$_3$). ESI-MS: m/z 504.4 (M+1), 526.5 (M+23). $C_{29}H_{21}N_5O_4$ [503.5].

Methyl

5-(benzyloxy)-8-((3'-cyano-[1,1'-biphenyl]-4-yl)amino)-6-oxo-5,6-dihydropyrido[2,3-*b*]pyrazine-7-carboxylate (**6c**): yellow solid, yield 64%, mp: 219-220 ℃. ^{1}H NMR (400 MHz, DMSO-d_6) δ9.72 (s, 1H, N-H), 8.89 (d, *J* = 2.4 Hz, 1H, pyrazine-H), 8.68 (d, *J* = 2.4 Hz, 1H, pyrazine-H), 8.20 (s, 1H, Ph-H), 8.06 (d, *J* = 8.0 Hz, 1H, Ph-H), 7.83 (d, *J* = 8.0 Hz, 1H, Ph-H), 7.77 (d, *J* = 8.6 Hz, 2H, Ph-H), 7.70 – 7.64 (m, 3H, Ph-H), 7.47 – 7.40 (m, 3H, Ph-H), 7.31 (d, *J* = 8.6 Hz, 2H, Ph-H), 5.18 (s, 2H, CH$_2$), 3.13 (s, 3H, CH$_3$). ESI-MS: m/z 504.4 (M+1), 526.5 (M+23), 542.5 (M+39). C$_{29}$H$_{21}$N$_5$O$_4$ [503.5].

Methyl

5-(benzyloxy)-8-((3'-cyano-[1,1'-biphenyl]-3-yl)amino)-6-oxo-5,6-dihydropyrido[2,3-*b*]pyrazine-7-carboxylate (**6d**): yellow solid, yield 78%, mp: 215-217 ℃. ^{1}H NMR (400 MHz, DMSO-d_6) δ 9.70 (s, 1H, N-H), 8.90 (d, *J* = 2.4 Hz, 1H, pyrazine-H), 8.69 (d, *J* = 2.4 Hz, 1H, pyrazine-H), 8.14 (s, 1H, Ph-H), 8.03 (d, *J* = 8.5 Hz, 1H, Ph-H), 7.86 (d, *J* = 7.7 Hz, 1H, Ph-H), 7.70 (t, *J* = 7.8 Hz, 1H, Ph-H), 7.65 (dd, *J* = 7.7, 1.6 Hz, 2H, Ph-H), 7.60 (d, *J* = 8.0 Hz, 1H, Ph-H), 7.55 (s, 1H, Ph-H), 7.50 (t, *J* = 7.8 Hz, 1H, Ph-H), 7.47 – 7.40 (m, 3H, Ph-H), 7.29 (d, *J* = 7.9 Hz, 1H, Ph-H), 5.19 (s, 2H, CH$_2$), 2.99 (s, 3H, CH$_3$). ESI-MS: m/z 504.4 (M+1), 526.5 (M+23), 542.5 (M+39). C$_{29}$H$_{21}$N$_5$O$_4$ [503.5].

Methyl

5-(benzyloxy)-6-oxo-8-((4-(pyrimidin-5-yl)phenyl)amino)-5,6-dihydropyrido[2,3-*b*]pyrazine-7-carboxylate (**6e**): yellow solid, yield 91%, mp: 198-199 ℃. ^{1}H NMR (400 MHz, DMSO-d_6) δ 9.77 (s, 1H, N-H), 9.18 (s, 3H, pyrimidine-H), 8.89 (d, *J* = 2.4 Hz, 1H, pyrazine-H), 8.68 (d, *J* = 2.4 Hz, 1H, pyrazine-H), 7.83 (d, *J* = 8.5 Hz, 2H, Ph-H), 7.65 (dd, *J* = 7.7, 1.6 Hz, 2H, Ph-H), 7.47 – 7.39 (m, 3H, Ph-H), 7.34 (d, *J* = 8.5 Hz, 2H, Ph-H), 5.18 (s, 2H, CH$_2$), 3.15 (s, 3H, CH$_3$). ^{13}C NMR (100 MHz, DMSO-d_6) δ 164.37, 157.12, 157.00, 154.44 (2×C), 146.49, 144.99, 144.62, 139.99, 138.54, 134.50, 132.54, 130.28, 129.55 (2×C), 128.93, 128.40 (2×C), 127.46, 127.07 (2×C), 124.66 (2×C), 102.89, 77.67, 51.47. ESI-MS: m/z 481.4 (M+1), 503.4 (M+23), 519.4 (M+39). C$_{26}$H$_{20}$N$_6$O$_4$ [480.5].

Methyl

5-(benzyloxy)-6-oxo-8-((3-(pyrimidin-5-yl)phenyl)amino)-5,6-dihydropyrido[2,3-*b*]p yrazine-7-carboxylate (**6f**): yellow solid, yield 70%, mp: 220-222 ℃. ^{1}H NMR (400 MHz, DMSO-*d*$_6$) δ 9.76 (s, 1H, N-H), 9.21 (s, 1H, pyrimidine-H), 9.14 (s, 2H, pyrimidine-H), 8.90 (d, *J* = 2.4 Hz, 1H, pyrazine-H), 8.69 (d, *J* = 2.4 Hz, 1H, pyrazine-H), 7.66 – 7.62 (m, 4H, Ph-H), 7.54 (t, *J* = 7.8 Hz, 1H, Ph-H), 7.47 – 7.39 (m, 3H, Ph-H), 7.37 – 7.31 (m, 1H, Ph-H), 5.19 (s, 2H, CH$_2$), 3.00 (s, 3H, CH$_3$). ^{13}C NMR (100 MHz, DMSO-*d*$_6$) δ 164.47, 157.51, 157.01, 154.65 (2×C), 146.54, 145.25, 144.59, 139.99, 138.54, 134.49, 134.00, 132.63, 129.85, 129.54 (2×C), 128.92, 128.39 (2×C), 127.39, 125.00, 123.69, 122.16, 102.60, 77.68, 51.15. ESI-MS: m/z 481.5 (M+1), 503.4 (M+23), 519.4 (M+39). C$_{26}$H$_{20}$N$_6$O$_4$ [480.5].

Methyl

5-(benzyloxy)-8-((3',4'-dimethoxy-[1,1'-biphenyl]-4-yl)amino)-6-oxo-5,6-dihydropyri do[2,3-*b*]pyrazine-7-carboxylate (**6g**): yellow solid, yield 60%, mp: 200-201 ℃. ^{1}H NMR (400 MHz, DMSO-*d*$_6$) δ 9.65 (s, 1H, N-H), 8.89 (d, *J* = 2.4 Hz, 1H, pyrazine-H), 8.67 (d, *J* = 2.4 Hz, 1H, pyrazine-H), 7.65 (d, *J* = 8.5 Hz, 4H, Ph-H), 7.47 – 7.41 (m, 3H, Ph-H), 7.25 – 7.21 (m, 4H, Ph-H), 7.04 (d, *J* = 8.2 Hz, 1H, Ph-H), 5.17 (s, 2H, CH$_2$), 3.86 (s, 3H, CH$_3$), 3.79 (s, 3H, CH$_3$), 3.11 (s, 3H, CH$_3$). ^{13}C NMR (100 MHz, DMSO-*d*$_6$) δ 164.40, 157.08, 149.10, 148.53, 146.42, 145.05, 144.55, 138.46, 137.62, 137.15, 134.52, 132.17, 129.53 (2×C), 128.92, 128.39 (2×C), 127.36, 126.34 (2×C), 124.91 (2×C), 118.63, 112.23, 110.11, 102.07, 77.65, 55.60 (2×C), 51.29. ESI-MS: m/z 539.5 (M+1), 561.4 (M+23), 577.4 (M+39). C$_{30}$H$_{26}$N$_4$O$_6$ [538.6].

Methyl

5-(benzyloxy)-8-((3',4'-dimethoxy-[1,1'-biphenyl]-3-yl)amino)-6-oxo-5,6-dihydropyri do[2,3-*b*]pyrazine-7-carboxylate (**6h**): yellow solid, yield 59%, mp: 159-161 ℃. ^{1}H NMR (400 MHz, DMSO-*d*$_6$) δ 9.64 (s, 1H, N-H), 8.89 (d, *J* = 2.4 Hz, 1H, pyrazine-H), 8.67 (d, *J* = 2.4 Hz, 1H, pyrazine-H), 7.65 (dd, *J* = 7.7, 1.6 Hz, 2H, Ph-H), 7.49 (d, *J* = 8.0 Hz, 1H, Ph-H), 7.47- 7.40 (m, 5H, Ph-H), 7.24 – 7.22 (m, 2H, Ph-H), 7.16 (d, *J* = 7.7 Hz, 1H, Ph-H), 7.05 (d, *J* = 8.4 Hz, 1H, Ph-H), 5.18 (s, 2H, CH$_2$), 3.85 (s, 3H, CH$_3$), 3.79 (s, 3H, CH$_3$), 3.02 (s, 3H, CH$_3$). ^{13}C NMR (100 MHz, DMSO-*d*$_6$) δ 164.40, 157.07, 149.03, 148.70, 146.45, 145.03, 144.58, 140.50, 139.27,

138.45, 134.52, 132.28, 129.53 (2×C), 129.21, 128.91, 128.38 (2×C), 127.35, 123.44, 122.94, 122.04, 118.85, 112.16, 110.37, 102.04, 77.65, 55.58 (2×C), 51.16. ESI-MS: m/z 539.6 (M+1), 561.4 (M+23), 577.4 (M+39). $C_{30}H_{26}N_4O_6$ [538.6].

Methyl 5-(benzyloxy)-8-(naphthalen-1-ylamino)-6-oxo-5,6-dihydropyrido[2,3-*b*]pyrazine-7-carboxylate (**6i**): yellow solid, yield 89%, mp: 213-214 ºC. ^{1}H NMR (400 MHz, DMSO-d_6) δ 9.71 (s, 1H, N-H), 8.92 (d, *J* = 2.4 Hz, 1H, pyrazine-H), 8.71 (d, *J* = 2.4 Hz, 1H, pyrazine-H), 8.01 – 7.94 (m, 2H, Ph-H), 7.90 (d, *J* = 8.2 Hz, 1H, Ph-H), 7.64 (dd, *J* = 7.7, 1.7 Hz, 2H, Ph-H), 7.59 – 7.49 (m, 3H, Ph-H), 7.47 – 7.41 (m, 3H, Ph-H), 7.38 (d, *J* = 7.3 Hz, 1H, Ph-H), 5.17 (s, 2H, CH2), 2.59 (s, 3H, CH3). ^{13}C NMR (100 MHz, DMSO-d_6) δ 164.15, 157.10, 146.39, 146.10, 144.40, 138.53, 134.65, 134.51, 133.78, 130.40, 129.53 (2×C), 128.92, 128.39 (2×C), 127.91, 127.23, 127.13, 126.39, 126.26, 125.29, 124.68, 123.53, 101.93, 77.68, 50.69. ESI-MS: m/z 453.5 (M+1), 475.4 (M+23). $C_{26}H_{20}N_4O_4$ [452.5].

Methyl 5-(benzyloxy)-8-(naphthalen-2-ylamino)-6-oxo-5,6-dihydropyrido[2,3-*b*]pyrazine-7-carboxylate (**6j**): yellow solid, yield 87%, mp: 185-186 ºC. ^{1}H NMR (400 MHz, DMSO-d_6) δ 9.79 (s, 1H, N-H), 8.90 (d, *J* = 2.3 Hz, 1H, pyrazine-H), 8.69 (d, *J* = 2.3 Hz, 1H, pyrazine-H), 7.92 – 7.90 (m, 2H, Ph-H), 7.83 (d, *J* = 7.7 Hz, 1H, Ph-H), 7.67 – 7.65 (m, 3H, Ph-H), 7.54 – 7.38 (m, 6H, Ph-H), 5.19 (s, 2H, CH2), 2.80 (s, 3H, CH3). ^{13}C NMR (100 MHz, DMSO-d_6) δ 164.39, 157.09, 146.48, 145.26, 144.58, 138.53, 136.63, 134.51, 132.88, 130.84 (2×C), 129.53, 128.92, 128.39 (2×C), 128.33, 127.56, 127.39 (2×C), 126.53, 125.60, 123.98, 121.27, 102.35, 77.67, 51.00. ESI-MS: m/z 453.5 (M+1), 475.4 (M+23), 491.4 (M+39). $C_{26}H_{20}N_4O_4$ [452.5].

Methyl 8-([1,1'-biphenyl]-4-ylamino)-5-(benzyloxy)-6-oxo-5,6-dihydropyrido[2,3-*b*]pyrazine-7-carboxylate (**6k**): yellow solid, yield 69%, mp: 185-187 ºC. ^{1}H NMR (400 MHz, DMSO-d_6) δ 9.69 (s, 1H, N-H), 8.89 (d, *J* = 2.4 Hz, 1H, pyrazine-H), 8.68 (d, *J* = 2.4 Hz, 1H, pyrazine-H), 7.70 – 7.64 (m, 6H, Ph-H), 7.49- 7.41 (m, 5H, Ph-H), 7.37 (t, *J* = 7.3 Hz, 1H, Ph-H), 7.28 (d, *J* = 8.5 Hz, 2H, Ph-H), 5.18 (s, 2H, CH2), 3.12 (s, 3H,

CH$_3$). ^{13}C NMR (100 MHz, DMSO-d_6) δ 164.38, 157.05, 146.43, 145.08, 144.56, 139.45, 138.48, 138.34, 137.12, 134.51, 129.53, 128.99, 128.91, 128.38, 127.40, 127.38, 126.76, 126.46, 124.92, 102.28, 77.65, 51.27. ESI-MS: m/z 479.5 (M+1), 501.5 (M+23), 517.4 (M+39). C$_{28}$H$_{22}$N$_4$O$_4$ [478.5].

4.1.6. General procedure for the synthesis of compounds **7a-7k**

Amides (**6a**–**6k**; 0.208 mmol) were dissolved in MeOH (5 mL) and CH$_2$Cl$_2$ (5 mL) and the solution degassed and stirred at room temperature under H$_2$ over 10% Pd $^\bullet$C (10% *w/w*, 2h). The mixture was filtered and the filtrate was concentrated, and the resulting residue were dissolved in MeOH and CH$_2$Cl$_2$, addition of *n*-hexane gave a precipitate, which was collected and dried to provide the target compounds (**7a**-**7k**).

Methyl 8-((4'-cyano-[1,1'-biphenyl]-4-yl)amino)-5-hydroxy-6-oxo-5,6-dihydropyrido[2,3-*b*]pyrazine-7-carboxylate (**7a**): yellow solid, yield 32%, mp: 262-264 ºC. ^{1}H NMR (400 MHz, DMSO-d_6) δ 10.98 (s, 1H, OH), 9.60 (s, 1H, N-H), 8.82 (d, *J* = 1.6 Hz, 1H, pyrazine-H), 8.68 (d, *J* = 1.6 Hz, 1H, pyrazine-H), 7.94-7.89 (m, 4H, Ph-H), 7.76 (d, *J* = 8.4 Hz, 2H, Ph-H), 7.29 (d, *J* = 8.4 Hz, 2H, Ph-H), 3.11 (s, 3H, CH$_3$). ^{13}C NMR (100 MHz, DMSO-d_6) δ 164.51, 157.60, 146.42, 144.96, 144.11, 143.88, 139.99, 137.90, 134.49, 132.88 (2×C), 127.23 (2×C), 127.19 (2×C), 126.86, 124.38 (2×C), 118.9, 109.77, 103.25, 51.32. ESI-MS: m/z 414.5 (M+1), 436.5 (M+23), 452.5 (M+39). C$_{22}$H$_{15}$N$_5$O$_4$ [413.4].

Methyl 8-((4'-cyano-[1,1'-biphenyl]-3-yl)amino)-5-hydroxy-6-oxo-5,6-dihydropyrido[2,3-*b*]pyrazine-7-carboxylate (**7b**): yellow solid, yield 61%, mp: 29-241 ºC. ^{1}H NMR (400 MHz, DMSO-d_6) δ 10.94 (s, 1H, OH), 9.55 (s, 1H, N-H), 8.83 (d, *J* = 2.2 Hz, 1H, pyrazine-H), 8.61 (d, *J* = 2.2 Hz, 1H, pyrazine-H), 7.94 (d, *J* = 8.4 Hz, 2H, Ph-H), 7.88 (d, *J* = 8.4 Hz, 2H, Ph-H), 7.57 (d, *J* = 7.8 Hz, 1H, Ph-H), 7.52 – 7.49 (m, 2H, Ph-H), 7.29 (d, *J* = 7.8 Hz, 1H, Ph-H), 2.97 (s, 3H, CH$_3$). ^{13}C NMR (100 MHz, DMSO-d_6) δ 164.59, 157.61, 146.42, 144.93, 144.39, 144.04, 139.91, 138.45, 137.84, 132.88 (2×C), 129.65, 127.47 (2×C), 126.83, 124.82, 123.73, 122.46, 118.84, 110.25, 102.78, 51.08. ESI-MS: m/z 414.5 (M+1). C$_{22}$H$_{15}$N$_5$O$_4$ [413.4].

Methyl

8-((3'-cyano-[1,1'-biphenyl]-4-yl)amino)-5-hydroxy-6-oxo-5,6-dihydropyrido[2,3-*b*]p

yrazine-7-carboxylate (**7c**): yellow solid, yield 54%, mp: 237-238 ºC. ^{1}H NMR (400

MHz, DMSO-*d*$_6$) δ 10.97 (s, 1H, OH), 9.57 (s, 1H, N-H), 8.83 (d, *J* = 1.8 Hz, 1H,

pyrazine-H), 8.61 (d, *J* = 1.8 Hz, 1H, pyrazine-H), 8.18 (s, 1H, Ph-H), 8.05 (d, *J* = 7.8

Hz, 1H, Ph-H), 7.82 (d, *J* = 7.8 Hz, 1H, Ph-H), 7.75 (d, *J* = 8.5 Hz, 2H, Ph-H), 7.67 (t,

J = 7.8 Hz, 1H, Ph-H), 7.28 (d, *J* = 8.5 Hz, 2H, Ph-H), 3.11 (s, 3H, CH$_3$). ^{13}C NMR

(100 MHz, DMSO-*d*$_6$) δ 164.55, 157.65, 146.43, 144.96, 144.16, 140.54, 139.57,

137.91, 134.43, 131.19 (2×C), 130.91 (2×C), 130.20, 129.92, 127.07, 126.86, 124.52,

118.85, 112.16, 103.07, 51.38. ESI-MS: m/z 414.4 (M+1), 436.4 (M+23), 452.5

(M+39). C$_{22}$H$_{15}$N$_5$O$_4$ [413.4].

Methyl

8-((3'-cyano-[1,1'-biphenyl]-3-yl)amino)-5-hydroxy-6-oxo-5,6-dihydropyrido[2,3-*b*]p

yrazine-7-carboxylate (**7d**): yellow solid, yield 60%, mp: 226-227 ºC. ^{1}H NMR (400

MHz, DMSO-*d*$_6$) δ 10.94 (s, 1H, OH), 9.53 (s, 1H, N-H), 8.83 (d, *J* = 2.3 Hz, 1H,

pyrazine-H), 8.61 (d, *J* = 2.3 Hz, 1H, pyrazine-H), 8.13 (s, 1H, Ph-H), 8.03 (d, *J* =

7.8 Hz, 1H, Ph-H), 7.85 (d, *J* = 7.8 Hz, 1H, Ph-H), 7.69 (t, *J* = 7.8 Hz, 1H, Ph-H),

7.58 – 7.47 (m, 3H, Ph-H), 7.27 (d, *J* = 8.5 Hz, 1H, Ph-H), 2.97 (s, 3H, CH$_3$). [13]C

NMR (101 MHz, DMSO-*d*$_6$) δ 164.62, 157.64, 146.43, 144.93, 144.39, 140.67,

139.86, 138.17, 137.85, 131.37, 131.26, 130.20, 130.18, 129.59, 126.83, 124.48,

123.60, 122.34, 118.78, 112.11, 102.74, 51.09. ESI-MS: m/z 414.4 (M+1), 431.5

(M+18), 436.5 (M+23), 452.5 (M+39). C$_{22}$H$_{15}$N$_5$O$_4$ [413.4].

Methyl

5-hydroxy-6-oxo-8-((4-(pyrimidin-5-yl)phenyl)amino)-5,6-dihydropyrido[2,3-*b*]pyraz

ine-7-carboxylate (**7e**): yellow solid, yield 57%, mp: 249-250 ºC. ^{1}H NMR (400 MHz,

DMSO-*d*$_6$) δ 10.99 (s, 1H, OH), 9.61 (s, 1H, N-H), 9.17 (s, 3H, pyrimidine-H), 8.83

(d, *J* = 2.0 Hz, 1H, pyrazine-H), 8.62 (d, *J* = 2.0 Hz, 1H, pyrazine-H), 7.82 (d, *J* = 8.4

Hz, 2H, Ph-H), 7.32 (d, *J* = 8.4 Hz, 2H, Ph-H), 3.13 (s, 3H, CH$_3$). ^{13}C NMR (100

MHz, DMSO-*d*$_6$) δ 164.54, 157.60, 157.07, 154.39(2×C), 146.42, 144.96, 144.07,

140.15, 137.88, 132.54, 130.01, 127.02 (2×C), 126.87, 124.47 (2×C), 103.30, 51.43.

ESI-MS: m/z 391.4 (M+1), 413.5 (M+23). $C_{19}H_{14}N_6O_4$ [390.4].

Methyl

5-hydroxy-6-oxo-8-((3-(pyrimidin-5-yl)phenyl)amino)-5,6-dihydropyrido[2,3-*b*]pyrazine-7-carboxylate (**7f**): yellow solid, yield 51%, mp: 223-224 ºC. ^{1}H NMR (400 MHz, DMSO-d_6) δ 10.98 (s, 1H, OH), 9.59 (s, 1H, N-H), 9.20 (s, 1H, pyrimidine -H), 9.13 (s, 2H, pyrimidine -H), 8.83 (d, *J* = 1.3 Hz, 1H, pyrazine-H), 8.62 (d, *J* = 1.1 Hz, 1H, pyrazine-H), 7.64 – 7.60 (m, 2H, Ph-H), 7.52 (t, *J* = 7.8 Hz, 1H, Ph-H), 7.32 (d, *J* = 7.7 Hz, 1H, Ph-H), 2.98 (s, 3H, CH$_3$). ^{13}C NMR (100 MHz, DMSO-d_6) δ 164.65, 157.61, 157.47, 154.63 (2×C), 146.46, 144.94, 144.39, 140.12, 137.87, 133.97, 132.66, 129.80, 126.83, 124.86, 123.48, 122.10, 102.93, 51.11. ESI-MS: m/z 391.4 (M+1), 413.5 (M+23), 429.4 (M+39). $C_{19}H_{14}N_6O_4$ [390.4].

Methyl

8-((3',4'-dimethoxy-[1,1'-biphenyl]-4-yl)amino)-5-hydroxy-6-oxo-5,6-dihydropyrido[2,3-*b*]pyrazine-7-carboxylate (**7g**): yellow solid, yield 52%, mp: 213-215 ºC. ^{1}H NMR (400 MHz, DMSO-d_6) δ 10.92 (s, 1H, OH), 9.46 (s, 1H, N-H), 8.82 (d, *J* = 2.0 Hz, 1H, pyrazine-H), 8.61 (d, *J* = 2.0 Hz, 1H, pyrazine-H), 7.64 (d, *J* = 8.5 Hz, 2H, Ph-H), 7.23 – 7.21 (m, 4H, Ph-H), 7.03 (d, *J* = 8.2 Hz, 1H, Ph-H), 3.86 (s, 3H, CH$_3$), 3.79 (s, 3H, CH$_3$), 3.10 (s, 3H, CH$_3$). ^{13}C NMR (100 MHz, DMSO-d_6) δ 164.56, 157.70, 149.10, 148.50, 146.35, 144.90, 144.19, 137.80, 137.77, 136.95, 132.20, 126.77, 126.31 (2×C), 124.80 (2×C), 118.59, 112.24, 110.12, 102.44, 55.60, 55.59, 51.25. ESI-MS: m/z 449.5 (M+1), 471.5 (M+23), 487.4 (M+39). $C_{23}H_{20}N_4O_6$ [448.4].

Methyl

8-((3',4'-dimethoxy-[1,1'-biphenyl]-3-yl)amino)-5-hydroxy-6-oxo-5,6-dihydropyrido[2,3-*b*]pyrazine-7-carboxylate (**7h**): yellow solid, yield 36%, mp: 165-166 ºC. ^{1}H NMR (400 MHz, DMSO-d_6) δ 10.96 (s, 1H, OH), 9.48 (s, 1H, N-H), 8.82 (d, *J* = 1.2 Hz, 1H, pyrazine-H), 8.61 (d, *J* = 1.2 Hz, 1H, pyrazine-H), 7.47 (d, *J* = 7.7 Hz, 1H, Ph-H), 7.42 – 7.38 (m, 2H, Ph-H), 7.23 – 7.19 (m, 2H, Ph-H), 7.14 (d, *J* = 7.7 Hz, 1H, Ph-H), 7.04 (d, *J* = 8.2 Hz, 1H, Ph-H), 3.84 (s, 3H, CH$_3$), 3.79 (s, 3H, CH$_3$), 3.00 (s, 2H, CH$_3$). ^{13}C NMR (100 MHz, DMSO-d_6) δ 164.58, 157.70, 149.03, 148.66, 146.40, 144.93, 144.21, 140.44, 139.42, 137.80, 132.32, 129.18, 126.79, 123.21, 122.82,

121.89, 118.82, 112.16, 110.34, 102.38, 55.57, 55.55, 51.11. ESI-MS: m/z 449.5 (M+1). $C_{23}H_{20}N_4O_6$ [448.4].

Methyl 5-hydroxy-8-(naphthalen-1-ylamino)-6-oxo-5,6-dihydropyrido[2,3-*b*]pyrazine-7-carb oxylate (**7i**): yellow solid, yield 62%, mp: 211-213 ºC. ^{1}H NMR (400 MHz, DMSO-d_6) δ 10.91 (s, 1H, OH), 9.51 (s, 1H, N-H), 8.85 (d, J = 1.4 Hz, 1H, pyrazine-H), 8.64 (d, J = 1.4 Hz, 1H, pyrazine-H), 7.98 (d, J = 7.7 Hz, 2H, Ph-H), 7.88 (d, J = 8.2 Hz, 1H, Ph-H), 7.76-7.47 (m, 3H, Ph-H), 7.36 (d, J = 7.2 Hz, 1H, Ph-H), 2.58 (s, 3H, CH$_3$). ^{13}C NMR (100 MHz, DMSO-d_6) δ 164.31, 157.73, 146.32, 145.28, 144.79, 137.88, 134.76, 133.79, 130.43, 127.91, 127.09, 126.54, 126.35, 126.23, 125.30, 124.68, 123.49, 102.29, 50.65. ESI-MS: m/z 363.4 (M+1), 385.4 (M+23). $C_{19}H_{14}N_4O_4$ [362.3].

Methyl 5-hydroxy-8-(naphthalen-2-ylamino)-6-oxo-5,6-dihydropyrido[2,3-*b*]pyrazine-7-carb oxylate (**7j**): yellow solid, yield 25%, mp: 212-214 ºC. ^{1}H NMR (400 MHz, DMSO-d_6) δ 10.97 (s, 1H, OH), 9.63 (s, 1H, N-H), 8.83 (d, J = 2.2 Hz, 1H, pyrazine-H), 8.62 (d, J = 2.2 Hz, 1H, pyrazine-H), 7.91- 7.88 (m, 2H, Ph-H), 7.81 (d, J = 7.7 Hz, 1H, Ph-H), 7.64 (s, 1H, Ph-H), 7.52 – 7.45 (m, 2H, Ph-H), 7.37 (dd, J = 8.7, 2.0 Hz, 1H, Ph-H), 2.79 (s, 3H, CH$_3$). ^{13}C NMR (100 MHz, DMSO-d_6) δ 164.57, 157.70, 146.42, 144.94, 144.38, 137.88, 136.78, 132.91, 130.74, 128.28, 127.54, 127.34, 126.82, 126.48, 125.49, 123.96, 121.09, 102.75, 50.98. ESI-MS: m/z 363.4 (M+1), 385.3 (M+23), 401.4 (M+39). $C_{19}H_{14}N_4O_4$ [362.3].

Methyl 8-([1,1'-biphenyl]-4-ylamino)-5-hydroxy-6-oxo-5,6-dihydropyrido[2,3-*b*]pyrazine-7-c arboxylate (**7k**): yellow solid, yield 35%, mp: 221-222 ºC. ^{1}H NMR (400 MHz, DMSO-d_6) δ 10.93 (s, 1H, OH), 9.50 (s, 1H, N-H), 8.82 (d, J = 2.2 Hz, 1H, pyrazine-H), 8.61 (d, J = 2.2 Hz, 1H, pyrazine-H), 7.69-7.64 (m, 4H, Ph-H), 7.47 (t, J = 7.6 Hz, 2H, Ph-H), 7.36 (t, J = 7.3 Hz, 1H, Ph-H), 7.26 (d, J = 8.4 Hz, 2H, Ph-H), 3.10 (s, 3H, CH$_3$). ^{13}C NMR (100 MHz, DMSO-d_6) δ 164.54, 157.67, 146.36, 144.91, 144.19, 139.47, 138.48, 137.82, 136.91, 128.96, 127.34, 126.78, 126.72, 126.42,

124.80, 102.64, 51.23. ESI-MS: m/z 389.4 (M+1), 411.4 (M+23), 427.4 (M+39). $C_{21}H_{16}N_4O_4$ [388.4].

4.2. HIV-1 RNase H inhibition assay

Wild-type (WT) HIV-1 BH10 reverse transcriptase (RT) was expressed in *E. coli* and purified as previously described [40, 41]. Synthetic oligonucleotides 31Trna (5´-UUUUUUUUUAGGAUACAUAUGGUUAAAGUAU-3´) and 21P (5´-ATACTTTAACCATATGTATCC-3´) were obtained from Sigma. The RNase H activity was determined using the template-primer 31Trna/21P [30]. The template RNA was labeled at its 5´ end with [γ-^{32}P] ATP (Perkin Elmer) and T4 polynucleotide kinase (New England Biolabs), and then purified with a mini Quick Spin^{TM} column (Roche). The labeled template was annealed to the 21-nt primer (21P) in 50 mM Tris-HCl (pH 8.0) containing 50 mM NaCl, as previously described [30]. RNase H cleavage assays were carried out for 20 s at 37 ºC with 20-40 nM HIV-1 RT in 30 µL of 50 mM Tris-HCl (pH 8.0), 50 mM NaCl, 5 mM $MgCl_2$, 25 nM ^{32}P-labeled template-primer (31Trna/21P), and 5% dimethyl sulfoxide (DMSO). The potential RNase H inhibitors were available in 50% DMSO. Appropriate dilutions of those drugs were preincubated with the RT for 5 min at 37 ºC in the assay buffer, and reactions were initiated by adding the labeled template-primer. Aliquots were removed at appropriate times and quenched with an equal volume of sample loading buffer [10 mM EDTA in 90% formamide containing xylene cyanol FF (3 mg/mL) and bromophenol blue (3 mg/mL)] and analyzed by denaturing polyacrylamide gel electrophoresis. The amounts of uncleaved substrate (31Trna) and products of 25 and 26 nucleotides were determined by phosphorimaging with a BAS1500 scanner (Fuji), using the program Tina version 2.09 (Raytest Isotopenmessgerate Gmbh, Staubenhardt, Germany). IC_{50} values (µM) were determined from dose-response curves after calculating the amount of cleaved substrate in the absence of inhibitor (5% DMSO) and in the presence of drug at concentrations in the range of 0.2 to 100 µM.

4.3. HIV-1 IN inhibition assay

HIV-1 IN inhibition assay was carried out using an ELISA method [31] and the XpressBio HIV-1 Integrase Assay Kit EZ-1700 (purchased from Suzhou Xishan

Biological technology co., LTD, China). Briefly, streptavidin-coated 96-well plates were coated with a double-stranded HIV-1 LTR U5 donor substrate (DS) DNA containing an end-labeled biotin for 30 min at 37 ℃. Full-length recombinant HIV-1 IN protein was then added, and the mixture incubated for another 30 min at 37 ℃. Test compounds were added to the enzyme reaction and incubated for 5 min at room temperature. Then a different double stranded target substrate (TS) DNA containing a 3'-end modification was added to the reaction mixture which was then incubated for 30 min at 37 ℃. The HIV-1 IN cleaves the terminal two bases from the exposed 3'-end of the HIV-1 LTR DS DNA and then catalyzes a strand-transfer recombination reaction to integrate the DS DNA into the TS DNA. The products of the reaction are detected spectrophotometrically using a horse radish peroxidase (HRP)-labeled antibody directed against the TS 3'-end modification. Therefore, HRP antibody solutions were added to the reaction and incubated during 30 min at 37 ℃. Following the incubation with the antibody, 100 µL of a 3,3',5,5'-tetramethylbenzidine (TMB) peroxidase substrate solution is added to each well and incubated for 10 minutes at room temperature. The reaction is stopped by adding 100 µL of the commercial TMB stop solution and the absorbance of the product is determined at 450 nm using a microtiter plate ELISA reader. The percentage inhibition obtained with the tested compounds was calculated by using the formula:

% Inhibition= [OD value with IN but without inhibitors – OD value with IN and inhibitors]/[OD value with IN and inhibitors – OD value without IN and inhibitors]

Inhibitory concentration 50% (µM) determined from dose−response curves.

4.4. In vitro anti-HIV assay

By using the MTT method described previously [42, 43], the synthesized compounds were evaluated for their activity against WT HIV-1 [44] (strain HIV-IIIB), and in MT-4 cells. At the beginning, stock solutions (10×final concentration) of test compounds were added at 25 µM volumes to two series of triplicate wells to allow simultaneous evaluation of their effects on mock and HIV-infected cells. Serial five-fold dilutions of the test compounds were made directly in flat-bottomed 96-well microtiter trays, including untreated control HIV-1 and mock-infected cells for each

sample, using a Biomek 3000 robot (Beckman instruments, Fullerton, CA). HIV-1 (IIIB) (50 μL at 100-300 $CCID_{50}$) (50% cell culture infectious dose) or culture medium were added to either the mock or HIV-infected wells of the microtiter tray. Mock-infected cells were used to evaluate the effect of test compounds on uninfected cells in order to assess their cytotoxicity. Exponentially growing MT-4 cells were centrifuged for 5 min at 1000 rpm and the supernatant was discarded. The MT-4 cells were resuspended at 6×10^5 cells/mL, and transferred 50 μL volumes to the microtiter tray wells. Five days after infection the viability of mock-and HIV-infected cells was determined spectrophotometrically. The MTT assay was based on the reduction of yellow colored 3(4,5-dimethylthiazol-2-yl)-2,5-diphenyltetrazolium bromide (MTT) (Acros Organics, Geel, Belgium) by mitochondrial dehydrogenase of metabolically active cells to a blue-purple formazan that can be measured spectrophotometrically. The absorbances were read in an eight-channel computer-controlled photometer (Multiscan Ascent Reader, Labsystems, Helsinki, Finland), at the wavelengths of 540 and 690 nm. All data were calculated using the median OD (optical density) value of two or three wells. The 50% effective antiviral concentration (EC_{50}) was defined as the concentration of the tested compound achieving 50% protection from viral cytopathicity. The 50% cytotoxic concentration (CC_{50}) was defined as the compound concentration that reduced the inability of mock-infected cells by 50%.

4.5. Molecular Docking

Molecular modeling of compounds **7a** and **7h** were performed using the Tripos molecular modeling packages Sybyl-X 2.0 [45]. Through the Tripos force field, **7a** and **7h** were optimized for 2000-generations till the maximum derivative of energy became 0.005 kcal/(mol*A). The flexible docking method (Surflex-Dock) docked the ligand automatically into the receptor ligand binding site by the use of protocol-based approach and empirically derived scoring function. The protein was prepared by removing the ligand, water molecules, and other unnecessary small molecules from the crystal structure of the ligand protein complex (PDB code: 5J1E for RNase H, 3OYA for IN) prior to docking; polar hydrogen atoms and charges were added to the protein. SurflexDock default settings were used for other parameters, such as the

maximum number of rotatable bonds per molecule (set to 100) and the maximum number of poses per ligand (set to 20). The atomic charges were recalculated using the Kollman all-atom approach for the protein and the Gasteig-Hückel approach for the ligand. And the binding interaction energy was calculated, including van der Waals, electrostatic, and torsional energy terms defined in the Tripos force field. After the protocol was generated, the optimized **7a** and **7h** were docked into the binding pockets and to define the binding interactions.

Conflict of interest

The authors declare no conflict of interest.

Acknowledgments

References:

[1] E. De Clercq, Antivirals: past, present and future, Biochem. Pharmacol. 85 (2013) 727-744.

[2] D. Kang, Z. Huo, G. Wu, J. Xu, P. Zhan, X. Liu, Novel fused pyrimidine and isoquinoline derivatives as potent HIV-1 NNRTIs: a patent evaluation of WO2016105532A1, WO2016105534A1 and WO2016105564A1, Expert. Opin. Ther. Pat. 27 (2017) 383-391.

[3] L. Menendez-Arias, Molecular basis of human immunodeficiency virus type 1 drug resistance: overview and recent developments, Antiviral Res. 98 (2013) 93-120.

[4] L. Menendez-Arias, D.D. Richman, Editorial overview: antivirals and resistance: advances and challenges ahead, Curr. Opin. Virol. 8 (2014) iv-vii.

[5] P. Zhan, C. Pannecouque, E. De Clercq, X. Liu, Anti-HIV Drug Discovery and Development: Current Innovations and Future Trends, J. Med. Chem. 59 (2016) 2849-2878.

[6] R. Costi, M. Metifiot, F. Esposito, G. Cuzzucoli Crucitti, L. Pescatori, A. Messore, L. Scipione, S. Tortorella, L. Zinzula, E. Novellino, Y. Pommier, E. Tramontano, C. Marchand, R. Di Santo, 6-(1-Benzyl-1H-pyrrol-2-yl)-2,4-dioxo-5-hexenoic acids as dual inhibitors of recombinant HIV-1 integrase and ribonuclease H, synthesized by a parallel synthesis approach, J. Med. Chem. 56 (2013) 8588-8598.

[7] L. Cao, W. Song, E. De Clercq, P. Zhan, X. Liu, Recent progress in the research of small molecule HIV-1 RNase H inhibitors, Curr. Med. Chem. 21 (2014) 1956-1967.

[8] X. Wang, P. Gao, L. Menendez-Arias, X. Liu, P. Zhan, Update on Recent Developments in Small Molecular HIV-1 RNase H Inhibitors (2013-2016): Opportunities and Challenges, Curr. Med. Chem. (2017) [Epub ahead of print].

[9] K. Klumpp, J.Q. Hang, S. Rajendran, Y. Yang, A. Derosier, P. Wong Kai In, H. Overton, K.E. Parkes, N. Cammack, J.A. Martin, Two-metal ion mechanism of RNA cleavage by HIV RNase H and mechanism-based design of selective HIV RNase H inhibitors, Nucleic Acids. Res. 31 (2003) 6852-6859.

[10] D.M. Himmel, S.G. Sarafianos, S. Dharmasena, M.M. Hossain, K. McCoy-Simandle, T. Ilina, A.D. Clark, Jr., J.L. Knight, J.G. Julias, P.K. Clark, K. Krogh-Jespersen, R.M. Levy, S.H. Hughes, M.A. Parniak, E. Arnold, HIV-1 reverse transcriptase structure with RNase H inhibitor dihydroxy benzoyl naphthyl hydrazone bound at a novel site, ACS Chem. Biol. 1 (2006) 702-712.

[11] E. Tramontano, F. Esposito, R. Badas, R. Di Santo, R. Costi, P. La Colla, 6-[1-(4-Fluorophenyl)methyl-1H-pyrrol-2-yl)]-2,4-dioxo-5-hexenoic acid ethyl ester a novel diketo acid derivative which selectively inhibits the HIV-1 viral replication in cell culture and the ribonuclease H activity in vitro, Antiviral Res. 65 (2005) 117-124.

[12] E.B. Lansdon, Q. Liu, S.A. Leavitt, M. Balakrishnan, J.K. Perry, C. Lancaster-Moyer, N. Kutty, X. Liu, N.H. Squires, W.J. Watkins, T.A. Kirschberg, Structural and binding analysis of pyrimidinol carboxylic acid and N-hydroxy quinazolinedione HIV-1 RNase H inhibitors, Antimicrob. Agents Chemother. 55 (2011) 2905-2915.

[13] P.D. Williams, D.D. Staas, S. Venkatraman, H.M. Loughran, R.D. Ruzek, T.M. Booth, T.A. Lyle, J.S. Wai, J.P. Vacca, B.P. Feuston, L.T. Ecto, J.A. Flynn, D.J. DiStefano, D.J. Hazuda, C.M. Bahnck, A.L. Himmelberger, G. Dornadula, R.C. Hrin, K.A. Stillmock, M.V. Witmer, M.D. Miller, J.A. Grobler, Potent and selective HIV-1 ribonuclease H inhibitors based on a 1-hydroxy-1,8-naphthyridin-2(1H)-one scaffold, Bioorg. Med. Chem. Lett. 20 (2010) 6754-6757.

[14] G.L. Beilhartz, M. Ngure, B.A. Johns, F. DeAnda, P. Gerondelis, M. Gotte, Inhibition of the ribonuclease H activity of HIV-1 reverse transcriptase by GSK5750 correlates with slow enzyme-inhibitor dissociation, J. Biol. Chem. 289 (2014) 16270-16277.

[15] J. Tang, F. Liu, E. Nagy, L. Miller, K.A. Kirby, D.J. Wilson, B. Wu, S.G. Sarafianos, M.A. Parniak, Z. Wang, 3-Hydroxypyrimidine-2,4-diones as Selective Active Site Inhibitors of HIV Reverse Transcriptase-Associated RNase H: Design, Synthesis, and Biochemical Evaluations, J. Med. Chem. 59 (2016) 2648-2659.

[16] S.K. Vernekar, Z. Liu, E. Nagy, L. Miller, K.A. Kirby, D.J. Wilson, J. Kankanala, S.G. Sarafianos, M.A. Parniak, Z. Wang, Design, synthesis, biochemical, and antiviral evaluations of C6 benzyl and C6 biarylmethyl substituted 2-hydroxylisoquinoline-1,3-diones: dual inhibition against HIV reverse transcriptase-associated RNase H and polymerase with antiviral activities, J. Med. Chem. 58 (2015) 651-664.

[17] J. Kankanala, K.A. Kirby, F. Liu, L. Miller, E. Nagy, D.J. Wilson, M.A. Parniak, S.G. Sarafianos, Z. Wang, Design, Synthesis, and Biological Evaluations of Hydroxypyridonecarboxylic Acids as Inhibitors of HIV Reverse Transcriptase Associated RNase H, J. Med. Chem. 59 (2016) 5051-5062.

[18] P. Gao, L. Zhang, L. Sun, T. Huang, J. Tan, J. Zhang, Z. Zhou, T. Zhao, L. Menendez-Arias, C. Pannecouque, E. Clercq, P. Zhan, X. Liu, 1-Hydroxypyrido[2,3-d]pyrimidin-2(1H)-ones as novel selective HIV integrase inhibitors obtained via privileged substructure-based compound libraries, Bioorg. Med. Chem. 25 (2017) 5779-5789.

[19] D. Kang, H. Zhang, Z. Zhou, B. Huang, L. Naesens, P. Zhan, X. Liu, First discovery of novel 3-hydroxy-quinazoline-2,4(1H,3H)-diones as specific anti-vaccinia and adenovirus agents via 'privileged scaffold' refining approach, Bioorg. Med. Chem. lett. 26 (2016) 5182-5186.

[20] Y. Song, W. Chen, D. Kang, Q. Zhang, P. Zhan, X. Liu, "Old friends in new guise": exploiting privileged structures for scaffold re-evolution/refining, Comb. Chem. High. Throughput. Screen.

17 (2014) 536-553.

[21] P. Cherepanov, G.N. Maertens, S. Hare, Structural insights into the retroviral DNA integration apparatus, Curr. Opin. Struct. Biol. 21 (2011) 249-256.

[22] L. Pescatori, M. Metifiot, S. Chung, T. Masoaka, G. Cuzzucoli Crucitti, A. Messore, G. Pupo, V.N. Madia, F. Saccoliti, L. Scipione, S. Tortorella, F.S. Di Leva, S. Cosconati, L. Marinelli, E. Novellino, S.F. Le Grice, Y. Pommier, C. Marchand, R. Costi, R. Di Santo, N-Substituted Quinolinonyl Diketo Acid Derivatives as HIV Integrase Strand Transfer Inhibitors and Their Activity against RNase H Function of Reverse Transcriptase, J. Med. Chem. 58 (2015) 4610-4623.

[23] J.F. Davies, 2nd, Z. Hostomska, Z. Hostomsky, S.R. Jordan, D.A. Matthews, Crystal structure of the ribonuclease H domain of HIV-1 reverse transcriptase, Science 252 (1991) 88-95.

[24] M. Billamboz, F. Bailly, M.L. Barreca, L. De Luca, J.F. Mouscadet, C. Calmels, M.L. Andreola, M. Witvrouw, F. Christ, Z. Debyser, P. Cotelle, Design, synthesis, and biological evaluation of a series of 2-hydroxyisoquinoline-1,3(2H,4H)-diones as dual inhibitors of human immunodeficiency virus type 1 integrase and the reverse transcriptase RNase H domain, J. Med. Chem. 51 (2008) 7717-7730.

[25] B.Y. Nguyen, R.D. Isaacs, H. Teppler, R.Y. Leavitt, P. Sklar, M. Iwamoto, L.A. Wenning, M.D. Miller, J. Chen, R. Kemp, W. Xu, R.A. Fromtling, J.P. Vacca, S.D. Young, M. Rowley, M.W. Lower, K.M. Gottesdiener, D.J. Hazuda, Raltegravir: the first HIV-1 integrase strand transfer inhibitor in the HIV armamentarium, Ann. N. Y. Acad. Sci. 1222 (2011) 83-89.

[26] E.D. Deeks, Elvitegravir: a review of its use in adults with HIV-1 infection, Drugs 74 (2014) 687-697.

[27] E. Ribera, D. Podzamczer, [Mechanisms of action, pharmacology and interactions of dolutegravir], Enferm. Infecc. Microbiol. Clin. 33 Suppl 1 (2015) 2-8.

[28] A. Markham, Bictegravir: First Global Approval, Drugs. 78 (2018) 601-606.

[29] X.Z. Zhao, S.J. Smith, M. Metifiot, B.C. Johnson, C. Marchand, Y. Pommier, S.H. Hughes, T.R. Burke, Jr., Bicyclic 1-hydroxy-2-oxo-1,2-dihydropyridine-3-carboxamide-containing HIV-1 integrase inhibitors having high antiviral potency against cells harboring raltegravir-resistant integrase mutants, J. Med. Chem. 57 (2014) 1573-1582.

[30] M. Alvarez, T. Matamoros, L. Menendez-Arias, Increased thermostability and fidelity of DNA synthesis of wild-type and mutant HIV-1 group O reverse transcriptases, J. Mol. Biol. 392

(2009) 872-884.

[31] Z. Debyser, P. Cherepanov, W. Pluymers, E. De Clercq, Assays for the evaluation of HIV-1 integrase inhibitors, Methods. Mol. Biol. 160 (2001) 139-155.

[32] G. Cuzzucoli Crucitti, M. Metifiot, L. Pescatori, A. Messore, V.N. Madia, G. Pupo, F. Saccoliti, L. Scipione, S. Tortorella, F. Esposito, A. Corona, M. Cadeddu, C. Marchand, Y. Pommier, E. Tramontano, R. Costi, R. Di Santo, Structure-activity relationship of pyrrolyl diketo acid derivatives as dual inhibitors of HIV-1 integrase and reverse transcriptase ribonuclease H domain, J. Med. Chem. 58 (2015) 1915-1928.

[33] M. Billamboz, F. Bailly, C. Lion, C. Calmels, M.L. Andreola, M. Witvrouw, F. Christ, Z. Debyser, L. De Luca, A. Chimirri, P. Cotelle, 2-hydroxyisoquinoline-1,3(2H,4H)-diones as inhibitors of HIV-1 integrase and reverse transcriptase RNase H domain: influence of the alkylation of position 4, Eur. J. Med. Chem. 46 (2011) 535-546.

[34] S. Hare, S.J. Smith, M. Métifiot, A. Jaxa-Chamiec, Y. Pommier, S.H. Hughes, P. Cherepanov, Structural and Functional Analyses of the Second-Generation Integrase Strand Transfer Inhibitor Dolutegravir (S/GSK1349572), Mol. Pharmacol. 80 (2011) 565.

[35] M. Metifiot, K. Maddali, B.C. Johnson, S. Hare, S.J. Smith, X.Z. Zhao, C. Marchand, T.R. Burke, Jr., S.H. Hughes, P. Cherepanov, Y. Pommier, Activities, crystal structures, and molecular dynamics of dihydro-1H-isoindole derivatives, inhibitors of HIV-1 integrase, ACS Chem. Biol. 8 (2013) 209-217.

[36] C. Bruhlmann, F. Ooms, P.A. Carrupt, B. Testa, M. Catto, F. Leonetti, C. Altomare, A. Carotti, Coumarins derivatives as dual inhibitors of acetylcholinesterase and monoamine oxidase, J. Med. Chem. 44 (2001) 3195-3198.

[37] J. Pretorius, S.F. Malan, N. Castagnoli, Jr., J.J. Bergh, J.P. Petzer, Dual inhibition of monoamine oxidase B and antagonism of the adenosine A(2A) receptor by (E,E)-8-(4-phenylbutadien-1-yl)caffeine analogues, Bioorg. Med. Chem. 16 (2008) 8676-8684.

[38] D. Altavilla, F. Squadrito, A. Bitto, F. Polito, B.P. Burnett, V. Di Stefano, L. Minutoli, Flavocoxid, a dual inhibitor of cyclooxygenase and 5-lipoxygenase, blunts pro-inflammatory phenotype activation in endotoxin-stimulated macrophages, Br. J. Pharmacol. 157 (2009) 1410-1418.

[39] S. Park, N. Chapuis, V. Bardet, J. Tamburini, N. Gallay, L. Willems, Z.A. Knight, K.M.

Shokat, N. Azar, F. Viguie, N. Ifrah, F. Dreyfus, P. Mayeux, C. Lacombe, D. Bouscary, PI-103, a dual inhibitor of Class IA phosphatidylinositide 3-kinase and mTOR, has antileukemic activity in AML, Leukemia. 22 (2008) 1698-1706.

[40] J. Boretto, S. Longhi, J.M. Navarro, B. Selmi, J. Sire, B. Canard, An integrated system to study multiply substituted human immunodeficiency virus type 1 reverse transcriptase, Anal. Biochem. 292 (2001) 139-147.

[41] T. Matamoros, J. Deval, C. Guerreiro, L. Mulard, B. Canard, L. Menendez-Arias, Suppression of multidrug-resistant HIV-1 reverse transcriptase primer unblocking activity by alpha-phosphate-modified thymidine analogues, J. Mol. Biol. 349 (2005) 451-463.

[42] R. Pauwels, J. Balzarini, M. Baba, R. Snoeck, D. Schols, P. Herdewijn, J. Desmyter, E. De Clercq, Rapid and automated tetrazolium-based colorimetric assay for the detection of anti-HIV compounds, J. Virol. Methods. 20 (1988) 309-321.

[43] C. Pannecouque, D. Daelemans, E. De Clercq, Tetrazolium-based colorimetric assay for the detection of HIV replication inhibitors: revisited 20 years later, Nat. Protoc. 3 (2008) 427-434.

[44] M. Popovic, M.G. Sarngadharan, E. Read, R.C. Gallo, Detection, isolation, and continuous production of cytopathic retroviruses (HTLV-III) from patients with AIDS and pre-AIDS, Science 224 (1984) 497-500.

[45] D. Kang, Z. Fang, B. Huang, X. Lu, H. Zhang, H. Xu, Z. Huo, Z. Zhou, Z. Yu, Q. Meng, G. Wu, X. Ding, Y. Tian, D. Daelemans, E. De Clercq, C. Pannecouque, P. Zhan, Structure-Based Optimization of Thiophene[3,2-d]pyrimidine Derivatives as Potent HIV-1 Non-nucleoside Reverse Transcriptase Inhibitors with Improved Potency against Resistance-Associated Variants, J. Med. Chem. 60 (2017) 4424-4443.

- A series of 5-hydroxypyrido[2,3-*b*]pyrazin-6(5*H*)-one derivatives as HIV-1 RNase H inhibitors were designed and synthesized for the first time.

- **7a** showed the better RNase H inhibitory activity than *β*-thujaplicinol.

- **7a** exhibited the best dual inhibitory activity against HIV-1 RNase H and IN.